RESPONSE OF SELF-CENTERING MASS PLYWOOD PANEL SHEAR WALLS

Rajendra Soti

Post-Doctoral Scholar
E-mail: sotir@oregonstate.edu

Arijit Sinha*†

Associate Professor
E-mail: arijit.sinha@oregonstate.edu

Ian Morrell†

Graduate Assistant
Department of Wood Science & Engineering
Oregon State University
Corvallis, OR 97331
E-mail: ian.morrell@oregonstate.edu

Byrne T. Miyamoto†

Structural Testing Cordinator
Tallwood Design Institute
Oregon State University
Corvallis, OR 97331
E-mail: Byrne.Miyamoto@oregonstate.edu

Abstract.   The rocking behavior of self-centering mass plywood panel (MPP) walls was investigated with and without the use of supplementary energy dissipation systems. Two energy dissipation systems were tested. The first system used a kinematically expanding hysteretic damper (KE-HD), whereas the second system used slip friction connections (SFCs). The reviewed energy dissipating systems were used in a self-centering system comprising one unbonded posttensioned (PT) hold-down rod on each side of the MPP walls. The cyclic performance of the PT and the hybrid MPP specimens was investigated through a series of full-scale quasi-static cyclic tests. The test results demonstrated the viability of the investigated energy dissipaters in self-centering MPP rocking systems. Results further indicate that hybrid specimens with SFC dissipate more energy and provide higher strength than those with KE-HDs, however, with higher residual drift.

Keywords: Kinematically expanding hysteretic damper (KE-HD), mass plywood panels (MPP), rocking walls, self-centering system, slip friction connections (SFCs).

INTRODUCTION AND BACKGROUND

Mass plywood panels (MPPs) are an engineered wood product made of several layers of face glued plywood. Figure 1 shows a section of MPP manufactured by a local manufacturer based in Oregon, USA. MPP wall panels generally have a combination of face and core panels. The plies in the face panels are oriented in a manner that allows the panel to have a higher axial stiffness in the longitudinal direction, whereas the core panels have orientations that increase the stability of the MPPs. Because MPP is a new product, extensive research is needed to ensure its structural performance for building applications in seismic regions.

There are only a few studies regarding the structural performance of MPPs. The authors were highly involved in development of the product and,

* Corresponding author
† SWST members

Figure 1.   Illustration of mass plywood panel.

therefore, were also the authors of other studies looking into "Connection Performance of MPPs" (in review) where component tests were performed to characterize three different fastener orientations and connection performance in MPPs. Recently, the rocking behavior of MPP shear walls was investigated through a series of quasi-static reverse cyclic tests and is reported in "Experimental Investigation of MPPs Shear Walls," (in review) by the same authors. The test results demonstrated the sensitivity of the lateral-load response of MPP to different base conditions. However, the rocking behavior of posttensioned (PT) MPP walls with and without the use of additional energy dissipation has not been explored.

The self-centering performance of shear wall panels is generally achieved through the use of bonded/unbonded PT tendons or bars. The posttensioning system allows structures to rock and return to its original position after an earthquake and minimizes structural damage. Rocking PT systems were originally implemented using prestressed concrete shear walls (Priestley 1991; Filiatrault et al 2004). Other researchers have investigated wood structures

with self-centering systems (Buchanan et al 2008; Sarti et al 2008; Kam et al 2010; Kuilen 2014; Smith et al 2014; Xia and van de 2014; Sarti et al 2016; Ganey et al 2016; Otero-Chans et al 2016; Sarti et al 2016; Akbas et al 2017; Fitzgerald (2019), Polastri et al 2019). The results from these studies showed self-centering performance with minimal structural damage to rocking walls. There is a current gap in the literature regarding the self-centering performance of PT MPP walls.

The PT tendons are designed to remain elastic for most events to provide the required restoring force. This is because inelasticity in the rod will reduce the restoring force and the self-centering. Because of the elastic design considerations, a system with only PT tendons will have low-energy dissipation in service; therefore, supplementary energy dissipating mechanisms are incorporated into most self-centering systems (Ganey et al 2016). A hybrid rocking system, consisting of PT and supplemental damping, is a stable and promising lateral force resisting system (Sarti et al 2015).

Several researchers have proposed supplemental dampers for wood structures. Examples include a kinematically expanding hysteretic damper (KE-HD) (Higgins 2001), tension-yielding steel rods (Palermo et al 2006; Smith et al 2007; Kramer et al 2016), U-shaped flexural plates (Kelly et al 1972; Baird et al 2014; Iqbal et al 2015; Ganey et al 2016, Zimmerman and Mcdonnell 2017), and slip friction connections (SFCs) (Loo et al 2014; Loo et al 2015; Hashemi et al 2018; Fitzgerald 2019).

Steel yielding replaceable fuse connectors are usually placed at the toes of rocking walls. They are designed so that the earthquake energy can be dissipated by plastic deformation of the fuse elements without producing structural damage to the shear walls (Palermo et al 2006; Smith et al 2007; Kramer et al 2016; Wang and Zhao 2018). These damaged connectors can be replaced, allowing for quick recovery after a seismic event.

Several types of SFCs have been proposed in self-centering systems. The SFC system typically consists of friction plates that slide relative to

each other. To develop the required friction, the sliding plates are clamped together with bolts and spring washers (Chancellor et al 2014). In these types of connections, energy is dissipated through frictional forces and relative sliding between sliding plates.

Research Objectives

This study investigates the hysteretic performance of PT MPP shear walls through displacement-controlled quasi-static cyclic testing. In the first phase of this study, the self-centering performance of PT-only specimens was investigated. In the second phase, a hybrid system using PT MPP walls and KE-HDs was tested (hybrid 1). Last, a second hybrid system using SFCs on PT MPP walls (hybrid 2) was investigated. The specific objectives of this study were as follows:

1. To gain an understanding of the self-centering performance of PT MPP rocking walls.
2. To determine the hysteretic response of a hybrid rocking configuration involving PT MPP walls and KE-HDs.
3. To investigate the hysteretic properties of PT MPP walls with SFCs.

MATERIALS AND METHODS

MPP for this study was produced from Freres Lumber Co. Inc. based in Lyons, OR, with a thickness of 76 mm. Figure 2 shows a list of components used to assemble self-centering and energy dissipation systems. Part 1 in Fig 2 is the restoring plate for the self-centering system connected to MPP walls, with a 25.4-mm diameter central hold-down rod (not shown in Fig 2), made with ASTM A193 B7 structural steel, and was mounted on each side of the MPP walls. The posttensioning of the hold-downs was achieved through Belleville washers (type 12-EH-168, made by Solon Manufacturing) and two nuts. Parts 2 through 4 in Fig 2 show Belleville washers, wood screws (ASSY 3.0 CSK 10 mm by 140 mm), and 45° wedge washers. Part 5 is the housing assembly for the KE-HD, allowing
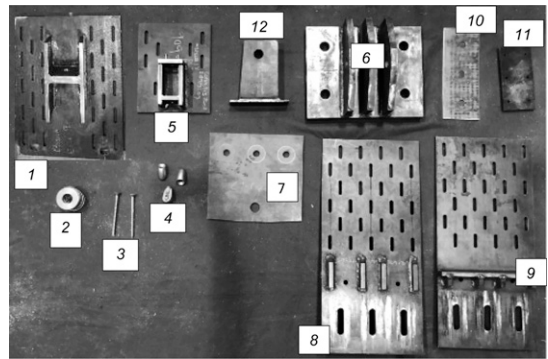

Figure 2. Several connection components: (1) slotted central restoring plate assembly, (2) Belleville washers, (3) screws (4) wedge washers, (5) housing for kinematically expanding hysteretic damper, (6) anchorage plate assembly, (7) cap plate, (8) slotted plate A, (9) slotted plate B, (10) brass shim, (11) HD polythene pad, and (12) bearing cog. Parts 6 to 12 are the components of slip friction connectors. All the parts except part 1 and part 6 were designed in Fitzgerald (2019).

connection to the wall. The details of this plate assembly are shown in Fig 3(b). All-thread 12.3-mm-diameter (ASTM A307 Gr. A) rods were used as the steel fuses. Parts 6 through 11 were used to assemble the SFC. Part 6 (Fig 2) was bolted and welded to the base rail. The SFC assembly, involving parts 6 through 11, is described in detail in the specimen descriptions section of this article. Parts 6 through 11 were originally designed by Fitzgerald (2019). Detail sketches of the restoring assembly and the SFC is provided in the Appendix as Figures A1 and A2, respectively.

The PT system uses a 91-cm hold-down rod centered on each side of the MPP walls. The advantage of this system is the simplified assembly because of easier accommodation of shorter rods. The Belleville washers were in series and were flattened before testing. This system allowed for a restoring tension force in the hold-down rods, even after yield. Until the deformation of the rod overcomes the initial displacement of flattening the Belleville washers, the PT system will have a tensile restoring force; yielding of the rod will reduce this force, however.

(a)

Left toe
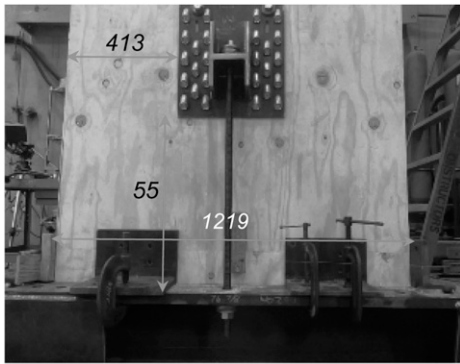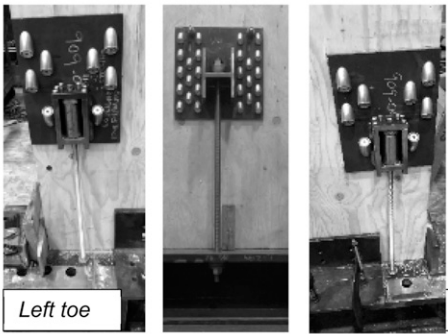
(b)
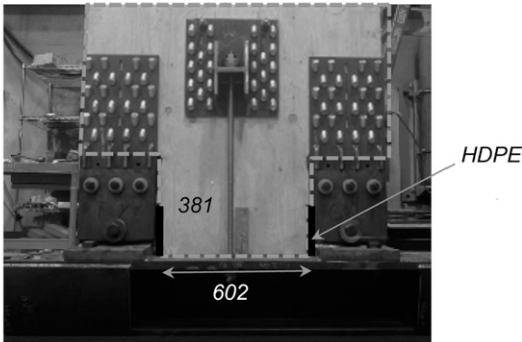
(c)

Figure 3. Details of specimens: (a) posttensioned specimen, (b) hybrid 1 specimen, and (c) hybrid 2 specimen.

EXPERIMENTAL PROGRAM

An experimental program was executed to investigate the hysteretic performance of PT MPP walls, with and without the use of supplementary energy dissipaters (Table 1). The first pair of MPP walls, PT specimens, had PT central hold-down rods running along each side of the MPP walls (Fig 3[a]). The second pair of walls, hybrid 1 specimens, had KE-HDs in addition to the central hold-down PT rods, as shown in Fig 3(b). Last, the third pair of walls, hybrid 2 specimens, were constructed with SFCs in addition to the central hold-down PT rods (Fig 3[c]). The specimens are described in details in the next section of this article.

PT Specimens

Figure 3(a) shows the front face of the PT specimens. These specimens had central hold-down PT bars on each side of the MPP specimens. The hold-down bars were prestressed between restoring plate assembly and steel footing beam using Belleville washers and nuts. A restoring plate assembly was connected to the MPP specimens using 45° CSK screws. The restoring plate assemblies were offset from the centerline of the wall by 6 mm on each side to avoid any conflict between the screws. When installed, the screws split the last ply of the MPP, causing slight bulging and splitting on the side opposite to the plate. The initial prestressing force of 178 kN was developed in the hold-downs using a torque wrench and a torque multiplier with a magnitude of 4, using calibration equation from Fitzgerald (2019). It is important to note that the torque value used on the PT rod in this study was higher than the values used in Fitzgerald (2019), and as such there may be a slight error in the torque to posttensioning conversion. To resist shear, steel angles were placed at each toe of the MPP walls. For assembly, the angle spacing was slightly wider than that of the wall and wedges were used to ensure force transfer with minimal slip throughout testing.

Table 1. Text matrix.

Specimen types	Number of repetitions	Self-centering system	Supplementary energy dissipater
Posttensioned	2	PT central hold-downs	—
Hybrid 1	2	PT central hold-downs	Kinematically expanding hysteric damper
Hybrid 2	2	PT central hold-downs	Slip friction connections

Hybrid 1 Specimens

These specimens were identical to PT specimens except two KE-HDs on each face of the MPP. The concept of the KE-HD from Higgins (2004) was modified to work with mass timber rocking walls. These connectors were installed at the corners of the MPP, as shown in Fig 3(b). The restoring plate assembly was connected to the MPP using the previously mentioned screws at 45°. The top end of the fuse connector was clamped with a pre-stressing chuck, whereas the bottom end was connected to the flange of the steel footing beam with nuts and washers on the top and bottom of the footing beam. This connection detail allowed the fuse to deform in tension, but slide in compression. As such, there was no pinching response in the fuse, as the prestressing chuck would slide down the rod during compression, always pulling on the same length of the material. To avoid the possible encounter of the diagonal screws, the housing for the fuses and prestressing chucks were offset 110 mm between the front and back faces.

Hybrid 2 Specimens

The third type of specimens makes use of SFCs. Unlike the two previous sets of specimens, 300 by 381-mm sections were removed from the corners of the MPP walls to accommodate the SFC. Figure 3(c) shows the SFC along with the geometry of these specimens. The assembly of the SFC is schematically illustrated in Fig 4. Full details of the connection design methodology can be found in Fitzgerald (2019), but important information and any differences are described in the following paragraphs. One of the only material changes between Fitzgerald (2019) and this study was to the anchorage plates, which was altered because of thickness differences between the three-ply cross-laminated timber (CLT) (105 mm) and the MPP used in this study (76 mm). In addition, the CSK screws used with the slotted plates were installed with an equal number of screws for tension and compression, 12 screws in each direction per plate.

One of the major differences between the hybrid 1 and hybrid 2 specimens is toe configuration. The SFC connection provided pin connection at toes
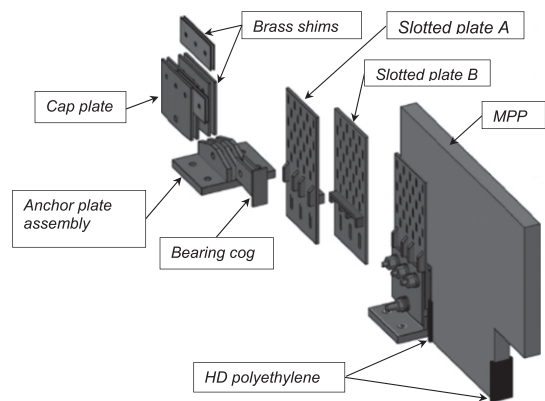

Figure 4.   Assembly of slip friction connection.

which maintains relatively consistent contact along the bearing surface. This is a contrast to the other specimens, which have a variable rocking point, which moves to maintain equilibrium between compression of the MPP and tension in metallic elements. Friction is developed in the SFC connection through Belleville washers clamping brass shims between the slotted plates and the cap plates (Fig 4). Each Belleville washer connection on the slotted plate consisted of three washers in parallel on one side of the plate and two in parallel on the other. This resulted in a group of three parallel washers in series with two parallel washers. The calibration equation presented by Fitzgerald (2019) was modified to take into account the washer layup presented in this study. Washers were torqued to a target value of 26 N-m to achieve an estimated target friction force of 105 kN for each toe. The other difference between the previous specimens and the hybrid 2 specimens was the shear transfer at the bottom of the wall. Rather than using angles located at the toes, two bearing cogs (Fig 4) connected the base of the wall to the anchorage plate, allowing the story shear force to transfer through the bearing. The bearing cogs were cut narrower than originally designed by Fitzgerald (2019) to accommodate the thinner wall.

Test Setup

Six (6) panels were tested under quasi-static cyclic loading. The typical test setup is shown

in Fig 5. A loading beam, consisting of two hollow structural sections welded together was connected to the actuator. The MPP was clamped between two plates attached to the loading beam, which allowed for minor variations in the position of the wall with respect to the actuator, facilitating load transfer from the actuator into the wall. Four Simpson Strong-tie HDQ8, hold-downs were connected to the upper portion of the wall. The hold-downs were then connected to the loading apparatus using all-thread rods and were tightened to hold the wall in-plane. In addition, on one side of the wall, pin–pin pipes were connected from the HDQ8 hold-downs to the parallel strong wall to provide out-of-plane bracing during testing. For the hybrid 1 specimens, the rods were placed in the prestressing chuck after the central hold-down bars were PT to ensure no accidental preload was placed on the energy dissipaters.

Instrumentation

Tests involved the use of the actuator load cell (300 kN) and linear variable displacement transducer (LVDT) (stroke: ±127 mm), as well as four other LVDTs attached near the base. An LVDT was attached to the centerline of the wall on the back face of the specimens. The instrumentation plan for all the wall types are shown in Fig 6. On each wall toe, an LVDT was attached on the back face of each wall specimen, measuring vertical deflection with respect to the base beam. This allowed for measurement of the uplift and the rotation of the wall specimens. The distances from the edge of the wall to the centerline of the vertical LVDTs were determined for each test to aid in the analysis.

In addition, an LVDT was attached in the middle of the front face of the specimens to measure the relative lateral displacement between the
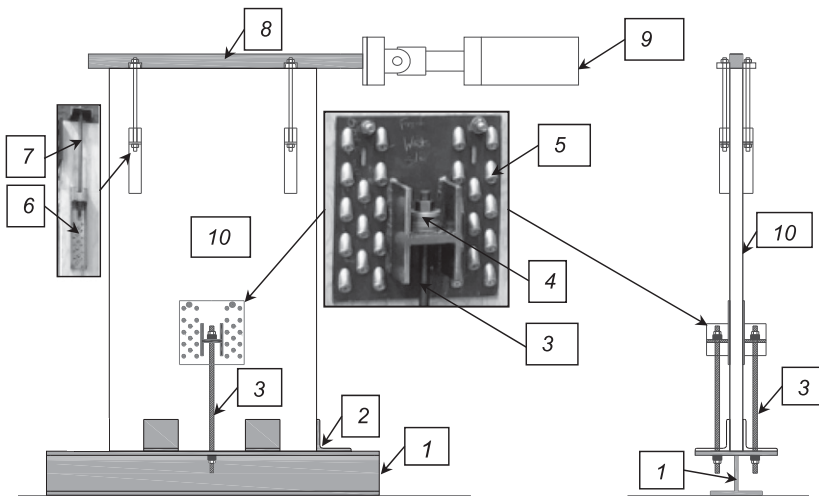
Legends:

1. Steel beam

2. Steel angle

3. Threaded rod (25.4 mm (ASTM A193 B7))

4. Belleville washer

5. 45 degree wedge washers

6. Simpson HDQ8 hold-down

7. Threaded rod (15.9 mm)

8. Loading arm

9. Actuator (300 kN, ± 127mm)

10. MPP panel (122 cm x 244 cmx7.62cm)

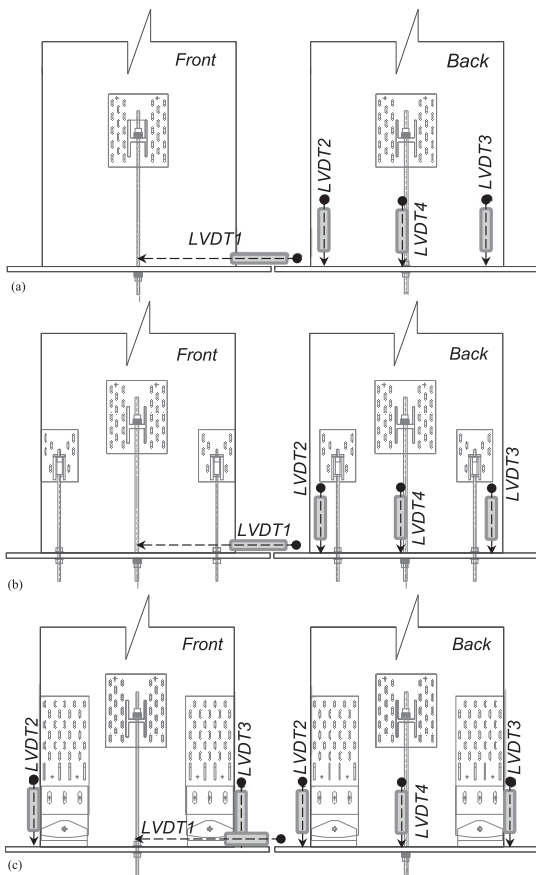Figure 5.   Test setup of the posttensioned specimen.

Figure 6.   The layout of sensors on mass plywood panel walls: (a) posttensioned only specimens, (b) hybrid 1 specimens, and (c) hybrid 2 specimens. The linear variable displacement transducer stands for linear displacement variable transducer.

Figure 7.   Loading protocol as per abbreviated CUREE protocol.

Lateral-Load Response

Figure 8 shows the experimental hysteretic response for each specimen, representing the force and deflection measured at the top of the wall. The load-deformation hysteresis response of the first PT specimen is shown in Fig 8(a). This specimen attained a peak load of 118 kN at 2.3% story drift. After this displacement, the strength suddenly dropped and regained slowly in trailing cycles. The second PT specimen achieved a peak load of 108 kN at 1.9% drift (Fig 8[b]). Both specimens had similar prepeak performance. However, the postpeak behavior between the two specimens was markedly different. This was due to the crushing behavior of the MPP as the second specimen underwent a buckling failure at the toes, explaining the sudden loss in strength and stiffness with minimal recovery. Based on the hysteresis of hybrid 1 specimens, it can be observed that the KE-HD bars did not noticeably influence the strength of PT specimens. However, a flag-shape hysteresis behavior was observed during the prepeak loading cycles (Fig 8[c] and [d]).

As evidenced by the lateral-load response in Fig 8 [e] and [f], the presence of SFC on hybrid 2 specimens improved the lateral-load resistance without strength degradation up to a 4% drift ratio. In PT and hybrid 1, the strength degraded at a point between 2.3% to 2.8% drift ratios. Both of the SFC PT specimens achieved a peak strength of approximately 175 kN, approximately 60 kN higher that of other types. As expected, hybrid 2

centerline of the wall and the floor. The displacement protocol used in this study was the abbreviated CUREE protocol (Krawinkler et al 2001) with a reference displacement of 38.1 mm, with a peak displacement amplitude of three times the CUREE reference displacement (Fig 7). Testing was conducted at a constant cyclic rate of 0.07 Hz.

RESULTS AND DISCUSSIONS

The test results of each group of specimens (PT, hybrid 1, and hybrid 2) were compared with the rocking performance and energy dissipation properties. Observations of strength, stiffness, and damage progression are discussed.
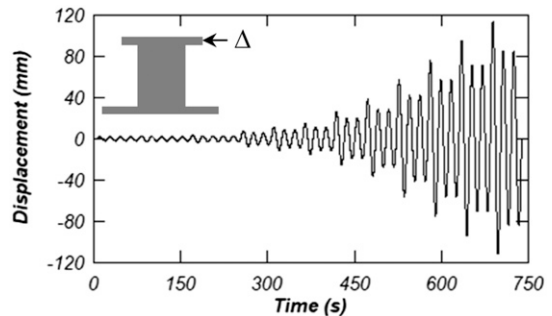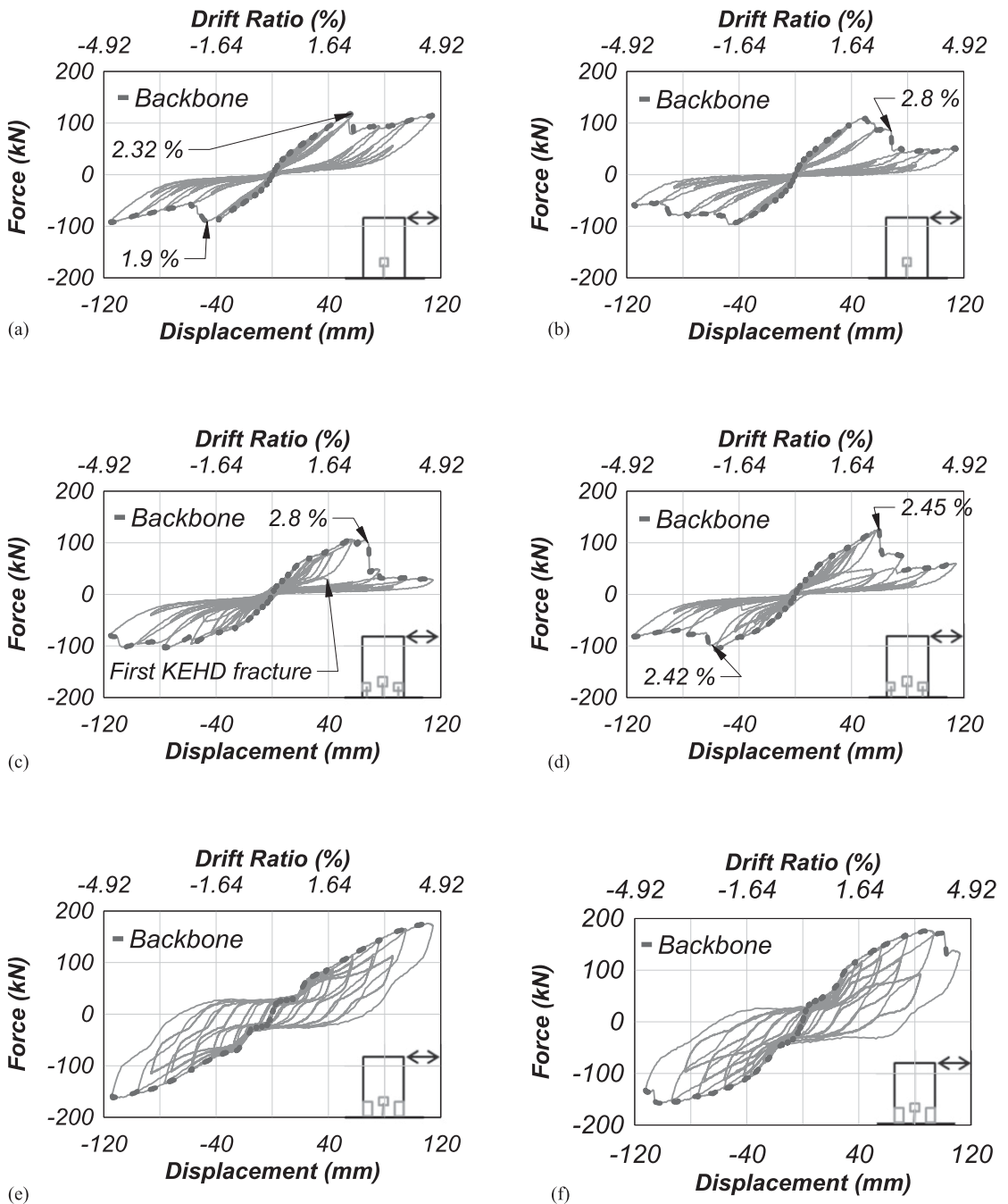
Figure 8. Hysteresis response of each specimen: (a) posttensioned (specimen 1), (b) PT (specimen 2), (c) hybrid 1 (specimen 1), (d) hybrid 1 (specimen 2), (d) hybrid 2 (specimen 1), and (e) hybrid 2 (specimen 2).

specimens showed stable hysteretic behavior with open hysteretic curves. These curves, however, were not as idealized flag-shaped because of friction in the SFC, slipping of the cap plates, and losses in the posttensioning force due to the yield of the steel components.

Self-Centering Performance

The residual drift of each specimen was determined as the drift of the specimen in a given cycle at zero force. Both the PT specimens demonstrated a self-centering characteristic with a maximum residual drift of 0.9% after 4% drift cycles (Table 2). It can be seen that both specimens recentered back to their original position. A similar trend can be observed in the hybrid 1 specimens. The observed maximum residual drift in these specimens was 0.4% after 4% drift. Hybrid 2 specimens exhibited a self-centered behavior; however, with a relatively higher amount of residual deformation. The observed residual drift after 2% drift cycle was 1.0%, and it increased up to 3.0% after 4% drift cycle (Table 2). Because the actuator linkage slack can be expected to be identical for all specimens, the higher residual drift in the hybrid 2 specimens was most likely caused by the friction between sliding plates and the extension of SFC.

Damage Progression

The PT and hybrid 1 specimens developed similar damage progression. The damage was concentrated at the toes, where crushing of MPP material occurred. The rapid strength degradation of these specimen was followed by the crushing failure of the toes. The typical failure mode observed in the PT specimens is illustrated in Fig

9(a). Although toe crushing was the dominant mode of failure, it occurred at substantially higher stress of 45 MPa as compared with 28 MPa (CLT) in Ganey et al (2016). This suggests a higher compressive strength of MPP parallel to the strong direction, but the value is calculated from theory and test results and was not directly measured. In addition to the crushing failure of MPP, tensile fracture of KE-HD was observed in the hybrid 1 specimen (Fig 9[b]). These specimens exhibited a flag-shape hysteretic behavior up until the fracture of the fuse connectors. However, because of the small diameter of the KE-HD rods, no adverse shock-loading effects were observed when the rods fractured. Unlike in other specimens, the hybrid 2 specimens did not develop compressive failure at the toes for a variety of reasons. First, the toes were confined by the SFC plates, resisting the local buckling failures previously noted in the PT and hybrid 1 tests, allowing for higher compressive force to be transferred from the wall into the bearing ledges of the SFC plate. Second, additional force transfer was available through the screws in the plate, further increasing the capacity of the toes. In the second specimen of hybrid 2 specimen, a vertical crack developed at approximately 4%, extending through the height of the specimen at where the routed section ended. This is indicative of the gross shear failure of MPP material. Although this is an undesirable failure mode, it occurred at a high story drift.

Backbone Curves

The experimentally obtained backbone curves are presented in Fig 10. These backbone curves were obtained from the envelope of the hysteresis in

Table 2.   Residual drift after the 2% and 4% drift cycles.

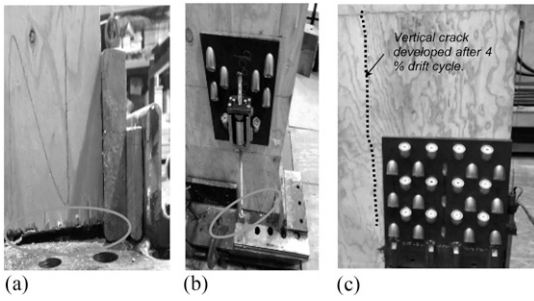| Specimen		After 2% drift cycle (%)		After 4% drift cycle (%)	
		Positive loading	Negative loading	Positive loading	Negative loading
Posttensioned	Specimen 1	0.07	−0.05	0.04	−0.06
	Specimen 2	0.08	−0.05	0.90	−0.09
Hybrid 1	Specimen 1	0.07	−0.14	0.40	−0.11
	Specimen 2	0.07	−0.05	0.20	−0.04
Hybrid 2	Specimen 1	1.06	−1.14	2.70	−2.50
	Specimen 2	0.93	−0.73	3.01	−2.50

Figure 9. The observed failure modes: (a) compression failure at toes of the PT specimen, (b) tensile failure of kinematically expanding hysteretic damper in hybrid 1 specimen, and (c) gross shear in the cross section failure in the mass plywood panel panels after 4% drift cycle.

both positive and negative directions. From these curves, all specimens exhibited approximately identical initial stiffness. However, the peak strength and the postpeak behavior varied significantly for different specimens. The PT and hybrid 1 specimens showed rapid strength degradation when compared with the backbone curves of hybrid 2 specimens. One of the hybrid 2 specimens did not show strength degradation during testing, as the other experienced a gross shear failure, as mentioned previously. The crushing of toes was the limiting failure condition for PT and hybrid 1 specimens, which capped the capacity of these specimens. In contrast, this crushing failure did not develop in the hybrid 2 specimens because of the presence of SFC at each toe of these specimens.

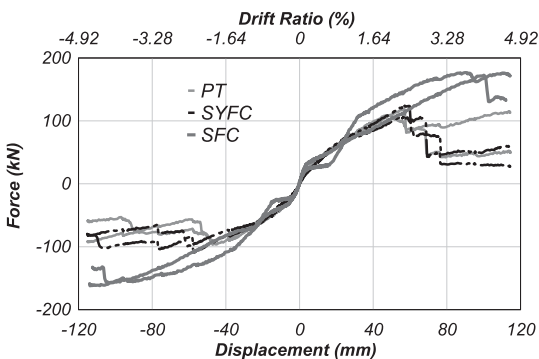Table 3 provides a summary of key parameters obtained from lateral-load responses for direct

Figure 10. Comparison of backbone curves.

comparison. These parameters were calculated using the ASCE 41-13 nonlinear static procedure trilinear curve. This trilinear curve determines yield and stiffness using an energy balance up to the peak load between the experimental curve and the trilinear curve as shown in Fig 11. The first branch of the trilinear curve is defined as the secant stiffness from the origin to 0.6 of the yield force, whereas the second branch is from the yield point to the peak force. The third branch of the trilinear curve takes the secant stiffness from the peak force to 0.6 of the yield force on the descending branch of the response. As this yield point is unknown during testing, not all specimens lost the capacity to reach 0.6 of the yield force. Therefore, the third branch was defined as the secant line between the peak force and postpeak point of lowest force in the backbone. The yield and peak strength values were larger for hybrid 2 specimens when compared with other groups of the specimen. This is mainly due to the avoidance of toe crushing in hybrid 2 specimens, the change in rocking point and the higher force developed in the SFC. The hybrid 2 specimens did, however, show smaller values of pre- and postyield stiffness. Although the hybrid 2 specimens achieved higher capacities, it is important to note that the peaks occurred at higher displacement values than in the other two specimen groups.

Energy Dissipation

The total energy dissipated by each specimen was determined by numerical integration using the trapezoidal rule on the force-displacement hysteresis loop. Figure 12 shows the cumulative energy dissipated during the duration of the test. The hybrid 1 specimen exhibited flag-shaped hysteresis performance, which was limited to the fracture of KE-HDs and yield of post-tensioning rod. As a result, the hybrid 1 specimens did show higher energy dissipation than the PT specimens, but the KE-HDs did not dissipate more energy than the crushing of the MPP. This can be inferred from the difference in the energy dissipated during the PT and hybrid 1 tests, as although there could be some difference due

Table 3.   Experimentally obtained properties of mass plywood panel panels.

Specimen		F_y (kN)	F_{max} (mm)	K (kN/mm)	$K_*\alpha_1$ (kN/mm)	$K_*\alpha_2$ (kN/mm)
Posttensioned	Specimen 1	38	119	4.67	1.67	−17.58
	Specimen 2	46	110	5.43	1.55	−2.13
Hybrid 1	Specimen 1	54	107	3.33	1.33	−3.57
	Specimen 2	53	124	3.79	1.64	−3.78
Hybrid 2	Specimen 1	97	176	2.44	1.11	−1.18
	Specimen 2	141	177	3.12	0.80	−3.14

F_y, yield force; F_{max}, maximum force; K, initial stiffness; α_1, postyield stiffness factor; α_1, postyield stiffness factor. The parameters presented in this table are defined in ASCE-41 nonlinear static procedure (ASCE/SEI 41-43 2014).

to MPP variation, the only major difference between these tests was the presence of the KE-HDs. Considering the idealized elastoplastic deformation of KE-HD, it appeared that the KE-HDs contributed about 20% of the total energy dissipation. The hybrid 2 specimens exhibited higher energy dissipation when compared with other groups of specimens. This is a result of a few factors. First, the hybrid 2 specimens both had higher force capacity and a lack of a crushing failure parallel to the grain, increasing the energy dissipated because of larger forces and less degradation. In addition, the reduced self-centering allowed for more open hysteretic behavior, further increasing the energy dissipation.

CONCLUSIONS

This study reports experimental results of PT MPP rocking walls with and without the use of supplementary energy dissipating systems. The energy dissipating systems comprised two different hybrid rocking systems: First, a hybrid system used KE-HDs, whereas the second system made use of SFCs at each bottom corner of the MPP. Self-centering was achieved through a central PT hold-down rod with Belleville washers on each face of the MPP. Based on the experimental results, the following conclusions can be drawn.

The proposed posttensioning system, using the Belleville washers, successfully provided the self-centering performance to the MPP walls.

The hybrid rocking system with KE-HDs as supplemental energy dissipaters dissipated energy through inelastic deformation of fuse connectors with self-centering performance. The hybrid 1 specimens resulted in a typical flag-shaped hysteretic behavior until the MPP crushing occurred. The KE-HDs began to fracture during the cycles
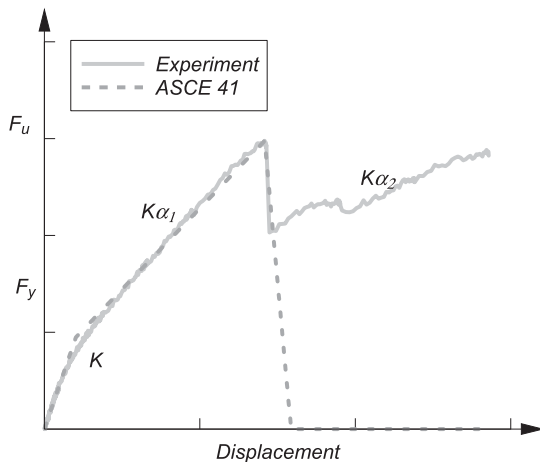

Figure 11.   Analysis of experimental data of posttensioned (specimen 1) based on ASCE-41 nonlinear static procedures.
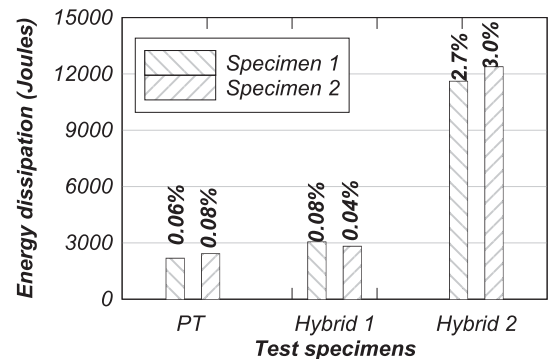

Figure 12.   Total energy dissipation of mass plywood panel walls. Percents above columns show residual story drift at 4% drift for comparison between energy dissipation and self-centering.

during and immediately after the MPP crushing. No adverse shock-loading effects were observed as a result of KE-HD fracture.

The SFC on hybrid 2 specimens successfully dissipated energy with symmetric hysteretic behavior common to friction devices without developing crushing failure at toes. The bearing cog in this connection successfully provided shear resistance against sliding. Unlike hybrid 1 specimens, hybrid 2 specimens exhibited higher residual drift values indicating the compromise in self-centering performance. This study reveals that both rocking performance and energy dissipation of MPP structures can be achieved by adding KE-HD or SFC to PT MPP walls.

REFERENCES

Akbas T, Sause R, Ricles JM, Ganey R, Berman J, Loftus S, Dolan JD, Pei S, van de Lindt JW, Blomgren HE (2017) Analytical and experimental lateral-load response of self-centering posttensioned CLT walls. J Struct Eng 143(6):04017019.

ASCE/SEI 41-43 (2014) Seismic rehabilitation of existing buildings. ASCE/SEI 41-13, Reston, VA.

ASTM A307 (2017) Standard specification for carbon steel bolts, studs, and threaded rod 60 000 PSI tensile strength. ASTM, West Conshohocken, PA.

ASTM A193 (2013) Standard specification for alloy-steel and stainless steel bolting for high temperature or high pressure service and other special purpose applications. ASTM, West Conshohocken, PA.

Baird A, Smith T, Palermo A, Pampanin S (2014) Experimental and numerical study of U-shape flexural plate (UFP) dissipators. NZSEE Conference, 21-23 March 2014, Auckland, NZ.

Buchanan A, Deam B, Fragiacomo M, Pampanin S, Palermo A (2008) Multi-storey prestressed timber buildings in New Zealand. Struct Eng Int 18(2):166-173.

Chancellor N, Eatherton M, Roke D, Akbaş T (2014) Self-centering seismic lateral force resisting systems: High performance structures for the city of tomorrow. Buildings 4(3):520-548.

Filiatrault A, Restrepo J, Christopoulos C (2004) Development of self-centering earthquake resisting systems. 13th World Conference on Earthquake Engineering, 1-6 August 2004, Vancouver, Canada.

Fitzgerald D (2019) Cross laminated timber shear wall with toe-screwed and slip friction connections. PhD dissertation, Oregon State University, Corvallis, OR.

Ganey R, Berman J, Yao L, Daniel Dolan J, Akbas T, Loftus S, Sause R, Ricles J, Pei S, Van De Lindt J, Blomgren H-E (2016) Experimental investigation of self-centering cross laminated timber walls. J Struct Eng 143(10):04017135.

Hashemi A, Zarnani P, Masoudnia R, Quenneville P (2018) Experimental testing of rocking cross laminated timber (CLT) walls with resilient slip friction (RSF) joints. J Struct Eng 144(1):04017180.

Higgins C (2001) Hysteretic dampers for wood frame shear walls. Proc. 2001 Structures Congress, 21-23 May 2001, Washington, D.C.

Iqbal A, Pampanin S, Palermo A, Buchanan AH (2015) Performance and design of LVL walls coupled with UFP dissipaters. J Earthquake Eng 19(3):383-409.

Kam WY, Pampanin S, Palermo A, Carr AJ (2010) Self-centering structural systems with combination of hysteretic and viscous energy dissipations. Earthq Eng Struct Dyn 39(10):1083-1108.

Kelly JM, Skinner RI, Heine AJ (1972) Mechanisms of energy absorption in special devices for use in earthquake resistant structures. Bull N Z Soc Earthq Eng 5(3):63-73.

Kramer A, Barbosa AR, Sinha A (2016) Performance of steel energy dissipators connected to cross-laminated timber wall panels subjected to tension and cyclic loading. J Struct Eng 142(4):E4015013.

Krawinkler H, Parisi F, Ibarra L, Ayoub A, Medina R (2001) Development of a testing protocol for woodframe structures. CUREE Publication No. W-02. Consortium of Universities for Research in Earthquake Engineering, Richmond, CA.

Loo WY, Kun C, Quenneville P, Chouw N (2014) Experimental testing of a rocking timber shear wall with slip-friction connectors. Earthq Eng Struct Dynm 43:1621-1639.

Loo WY, Quenneville P, Chouw N (2015) Rocking timber structure with slip-friction connectors conceptualized as a plastically deformable hinge within a multistory shear wall. J Struct Eng 142(4):E4015010.

Otero-Chans D, Estévez-Cimadevila J, Martín-Gutiérrez E, Pérez-Valcárcel J (2016) Application of a new system of self-tensioning to the design of large-span wood floor framings. J Struct Eng 142(6):04016012.

Palermo A, Pampanin S, Buchanan A (2006) Experimental investigations on LVL seismic resistant wall and frame subassemblies. First European Conference on Earthquake Engineering and Seismology, 3-8 September 2006, Geneva, Switzerland.

Polastri A, Izzi M, Pozza L, Loss C, Smith I (2019) Seismic analysis of multi-story timber buildings braced with a CLT

core and perimeter shear-walls. Bull Earthquake Eng 17(2):1009-1028.

Priestley MJN (1991) Overview of PRESSS research program. PCI J 36(4):50-57.

Sarti F, Palermo A, Pampanin S (2008) Simplified design procedures for post-tensioned seismic resistant timber walls. 15th World Conference of Earthquake Engineering, Lisbon, Portugal.

Sarti F, Palermo A, Pampanin S (2015) Quasi-static cyclic testing of two-thirds scale unbonded posttensioned rocking dissipative timber walls. J Struct Eng 142(4):E4015005.

Sarti F, Palermo A, Pampanin S (2016) Development and testing of an alternative dissipative posttensioned rocking timber wall with boundary columns. J Struct Eng 142(4): E4015011.

Smith TJ, Ludwig F, Pampanin S, Fragiacomo M, Buchanan A, Deam B, Palermo A (2007) Seismic response of hybrid-LVL coupled walls under quasi-static and pseudo-dynamic testing. New Zealand Society for Earthquake Engineering Conference, 30 March-1 April 2007, Palmerston North, New Zealand.

Smith T, Ponzo FC, Di Cesare A, Pampanin S, Carradine D, Buchanan AH, Nigro D (2014) Post-tensioned glulam beam-column joints with advanced damping systems: Testing and numerical analysis. J Earthquake Eng 18(1): 147-167.

Wang J, Zhao H (2018) High performance damage-resistant seismic resistant structural systems for sustainable and resilient city: A review. Shock Vib 18:1-32.

Xia Z, van de Kuilen JWG (2014) Lateral behavior of post-tensioned cross laminated timber walls using finite element analysis. World Conference on Timber Engineering, 10-14 August 2014, Quebec City, Canada.

Zimmerman RB, Mcdonnell E (2017) Framework - A tall re-centering mass timber building in the United States. 2017 NZSEE Conference, 27-29 April 2017, Wellington, NZ.

APPENDIX
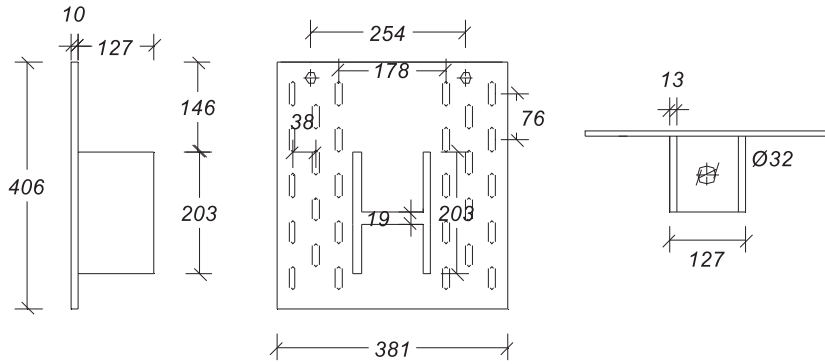
(a)
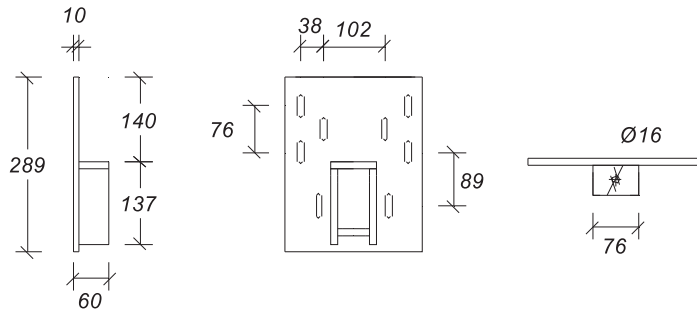
(b)

Figure A1.   Details of restoring plates: (a) central restoring plate assembly (part 1 in Fig 2) and (b) plate to house KE-HD assembly (part 5 in Fig 2). Dimensions are in mm.
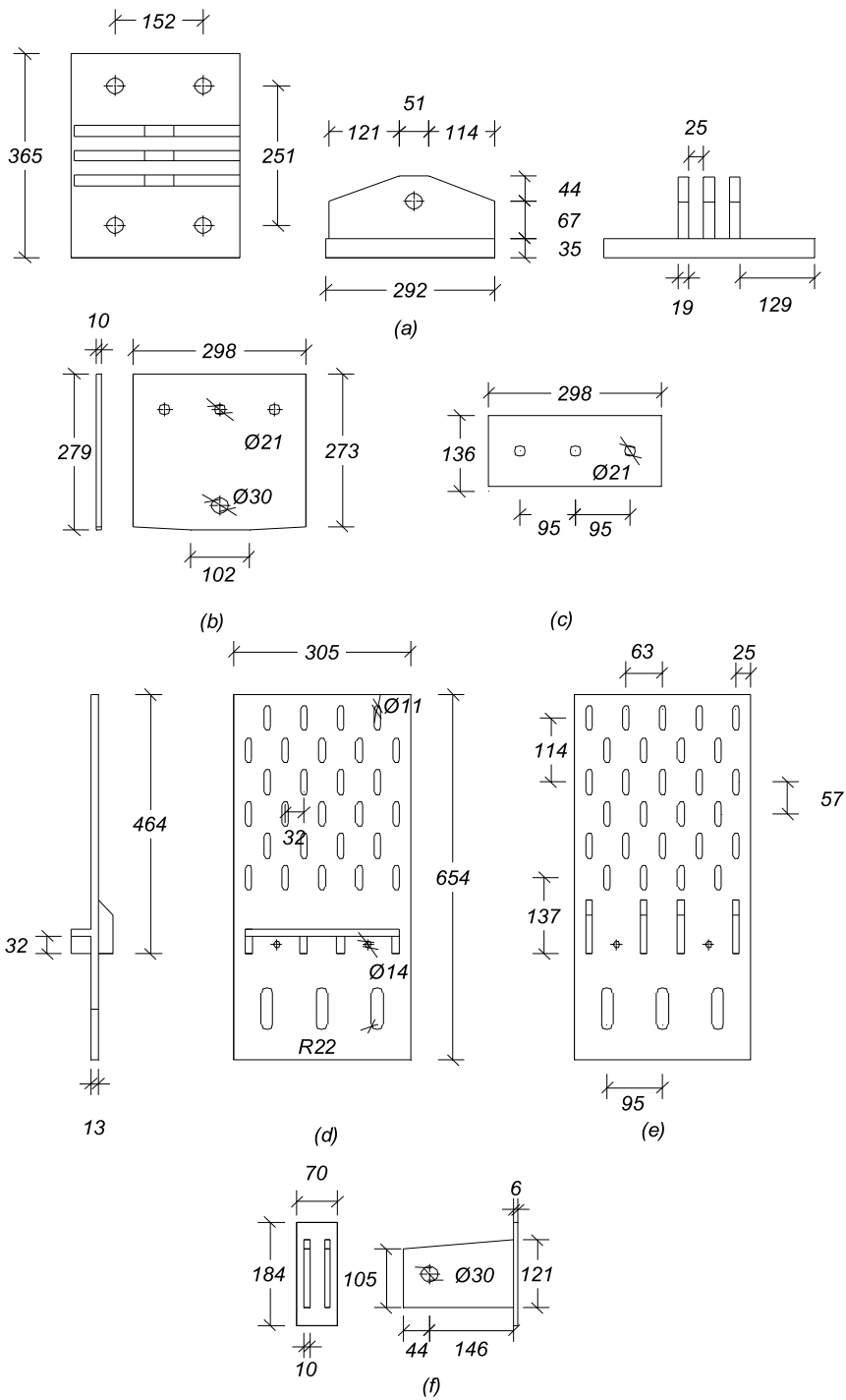
Figure A2.   Slip friction connection details: (a) anchor plate assembly, (b) cap plate details, (c) brass shim, (d) slotted plate A, (e) slotted plate B, and (f) bearing cog. Dimensions are in mm.